Journal of MATERIALS RESEARCH

Article
DOI: 10.1557/jmr.2018.481

Protein-functionalized WO_3 nanorods–based impedimetric platform for sensitive and label-free detection of a cardiac biomarker

Deepika Sandil[1], Suresh C. Sharma[2], Nitin K. Puri[2,a)]

[1]Advanced Sensor Laboratory, Department of Applied Physics, Delhi Technological University, Delhi 110042, India; and Department of Applied Physics, Bhagwan Parshuram Institute of Technology, Delhi 110089, India
[2]Advanced Sensor Laboratory, Department of Applied Physics, Delhi Technological University, Delhi 110042, India
[a)]Address all correspondence to this author. e-mail: nitinkumarpuri@dtu.ac.in, nitinpuri2002@yahoo.co.in

Received: 6 September 2018; accepted: 26 November 2018

We report the development of a sensitive and a label-free electrochemical immunosensing platform for the detection of cardiac biomarker troponin I (cTnI) using tungsten trioxide nanorods (WO_3 NRs). The low-temperature hydrothermal technique was employed for the controlled synthesis of WO_3 NRs. Thin films of 3-aminopropyltriethoxy saline (APTES)-functionalized WO_3 NRs were deposited on indium tin oxide (ITO)-coated glass substrate (0.5 cm × 1 cm) using electrophoretic deposition technique. The covalent immobilization of cTnI antibody onto functionalized WO_3 NRs electrode was accomplished using EDC-NHS [1-(3-(dimethylamino)-propyl)-3-ethylcarbodiimide hydrochloride and *N*-hydroxysulfosuccinimide] chemistry. The structural and morphological characterizations of WO_3 NRs and functionalized WO_3 NRs were studied using X-ray diffraction, field emission scanning electron microscopy, transmission electron microscopy, Fourier transform infrared spectroscopy, and electrochemical techniques. The impedimetric response study of the proposed immunosensor demonstrates high sensitivity [6.81 KΩ mL·cm^2)] in a linear detection range of 0.01–10 ng/mL. The excellent selectivity, good reproducibility, and long-term stability of the proposed immunosensing platform indicate WO_3 NRs as a suitable platform for the development of a point-of-care biosensing device for cardiac detection.

Introduction

In recent times, nanotechnology-based research has uncovered a multitude of novel materials suitable for the designing of biosensors. Among the numerous nanomaterials, metal oxide–based nanomaterials have been considered significant due to their great efficacy, nontoxicity, functional biocompatibility, and catalytic behavior [1, 2]. And among different morphologies, one-dimensional (1D) materials such as nanowires, nanorods, and nanofibers possess distinct features, such as enhanced electronic properties, unique catalytic activities, and high surface area. Such excellent properties of 1D material make it a promising platform for the development of biosensors by providing high signal-to-noise ratio, higher sensitivity, large surface area, and shorter response time [3, 4, 5, 6]. Recently, Augustine et al. have developed the 1D metal oxide–based platform for cancer detection [7]. Zhao et al. had developed ZnO nanowire–based electrochemical biosensor for L-lactic acid amperometric detection [8]. All these results indicate that 1D metal oxide–based materials can be ideal candidates for the development of sensitive biosensors.

The nanostructured tungsten trioxide (nWO_3) is an *n*-type semiconductor and has gained increasing attentions due to its potential in various fields such as electrochromic devices, photo-oxidation, solar cell devices, and sensors [9, 10, 11, 12]. It belongs to the family of transition metal oxide with electronic conformations of d^0 and d^{10}, which exhibits stimulating characteristics and steadiness important for the sensing uses. High electroactive surface area, fast electron transfer kinetics, and enhanced electrochemical properties are some of the important characteristics of nWO_3 that makes it an ideal candidate as a sensing electrode [13, 14, 15]. Owing to these exclusive electrochemical properties, nWO_3 can be considered as an ideal platform for sensing applications. Zhou et al. demonstrated the use of Na-doped tungsten trioxide

nanorods (WO_3 NRs) as a sensing platform for the detection of BPA [16]. Santos et al. fabricated nitrite biosensor based on WO_3 nanoparticles [14]. Indeed, the versatile properties of nWO_3, such as high sensitivity, biocompatibility, and reversible kinetics, make nWO_3 as a promising platform for the construction of biosensing electrodes. WO_3 nanostructures, such as nanorods, nanofibers, and nanobelts, have shown remarkable performance by providing high electrical and thermal electron transport kinetics due to the quantum confinement along with flexibility that can enable the physical manipulation of its structure. Also, electrical conductivity of these highly confined structures becomes very sensitive to the presence of ions and other carriers [17]. In this work, we report the synthesis of hexagonal phase WO_3 NRs using a facile hydrothermal method. And as-synthesized WO_3 NRs were used as an immobilized matrix for the fabrication of biosensing platform.

Acute myocardial infarction (AMI) is one of the severe cardiac vascular diseases. Bad cholesterol, saturated fats, trans-fat, and high blood pressure are few of the leading causes of the AMI. Different conventional methods have been in use for the detection of AMI, including enzyme-linked immunosorbent assay (ELISA), radioimmunoassay, and fluoroimmunoassay. However, these methods are complex, expensive, and time-consuming and need experts for the analysis. The biosensor in this regard can be seen as an alternative technique for the detection of AMI diseases as it offers simplicity in processing, low cost, high sensitivity, small sample volume, and portability [18]. It confers the exquisite specificity and sensitiveness of biomolecules in conjunction with a physicochemical transducer, which carries out the biointeraction measurements with real-time, ease, and simple-to-use formats. Among the various studied biosensors, such as optical, electrical, and electrochemical, the electrochemical immunosensors are gaining significant attention as a label-free, fast, portable, and reliable analytical tool for clinical diagnostics and environmental monitoring and in health care [19, 20, 21]. The electrochemical immunosensors are based on specific antigen–antibody interaction and considered as a most sensitive detection tool in diagnosis because of its fast driven analysis, simplicity in its functioning, precise measurement, and ease of fabrication. For successful development of an electrochemical immunosensor, the immobilization of biomolecules and amplification of response signal are the primary requisite [22]. Nanostructured metal oxides in this context have been preferred as an immobilized matrix due to their strong adherence behavior, chemical stability, and high catalytic activity [1, 2, 22].

Cardiac biomarkers are known to play a significant role in the development of biosensors as point-of-care (POC) devices [23]. They are used in the diagnosis of AMI by detecting the myocardial damage in the cells. These cardiac biomarkers are helpful in the diagnosis of the patient with ischemic chest pain not only with diagnostic ECG but also with non-diagnostic ECG. Among different cardiac biomarkers studied, myoglobin (Mb), creatine kinase-MB (CK-MB) isoenzyme, and cardiac troponin I (cTnI) have been found to be specific biomarkers present only in cardiac muscles. However, cardiospecificity of cTnI and long persistence of it in the blood circulation make it a principal biochemical marker of the cardiac injury [24, 25]. cTnI is a protein with a molecular weight of 29 kDa and is one of the subunits of troponin complex present in cardiac muscles. It gets released into the blood serum within 3–5 h after the onset of cardiac injury, crossing the normal limit value of the healthy humans (<0.5 ng/mL) and remains elevated for 6–10 days. The concentration of cTnI in patients ranging from 0.6 to 1 ng/mL indicates minor damage to the cells, whereas more than 1 ng/mL remarks the risk for future heart injuries. Thus, monitoring the concentration of cTnI in serum at an early stage will be clinically significant as the diagnostic tool [26].

Here, we demonstrate the application of WO_3 NR–based immunosensing platform for the label-free electrochemical detection of cardiac biomarker. The structural and electrochemical characteristics of the fabricated platform have been characterized using various spectroscopic techniques. Through this work, the author has strived to present the suitability and applications of nWO_3 in the field of biosensing.

Results and discussions

Microscopic and structural studies

The crystallinity of the hydrothermally synthesized WO_3NRs was studied using X-ray diffraction (XRD) pattern, as shown in Fig. 1. The high-intense diffraction peaks observed at two-theta value 23.1°, 28.22°, 36.75°, 49.8°, and 56.2° correspond to (002), (200), (202), (220), and (204) crystal planes of WO_3 of

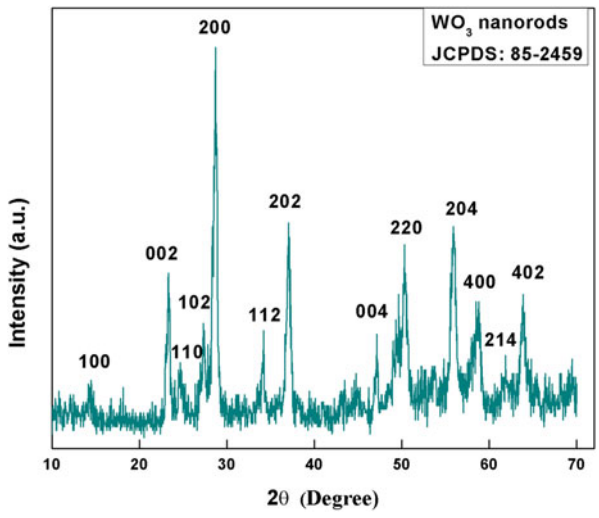

Figure 1: XRD pattern of hydrothermally synthesized nWO_3.

hexagonal phase, respectively. The other major diffraction peaks observed at 14.01°, 24.3°, 27.2°, 33.8°, 47.4°, 58.12°, 61.98°, and 63.45° correspond to (100), (110), (102), (112), (004), (400), (214), and (402) crystal planes, respectively, indicating the formation of pure hexagonal WO_3 phase (JCPDS 85-2459). The average crystallite size of WO_3 NRs was calculated using the Debye–Scherrer's equation given as follows:

$$d = 0.89\lambda/\beta\cos\theta \quad , \tag{1}$$

where λ (1.540 Å) corresponds to X-ray wavelength and β and θ represent full width at half maximum and Bragg's angle, respectively. The calculated crystallite size of WO_3 NRs was found to be 68 nm.

Figure 2 represents the micrographs depicting the morphological structure of the synthesized WO_3 sample, as examined under a field emission scanning electron microscope (FESEM) and transmission electron microscope (TEM). FESEM micrograph observed at low magnification [Fig. 2(a)] revealed that the synthesized sample has a morphological structure of nanorods grown in large scale, and at high magnification [Fig. 2(b)], we observed existence of nanorods bundles with inhomogeneous distribution. The estimated diameter of these nanorods was found as 50 ± 30 nm. The selected area electron diffraction [Fig. 2(c)] pattern showed that the synthesized WO_3 NRs were single crystalline and grown along [002], [112], and [204] directions. These results were in good agreement with the XRD studies. The TEM image [inset, Fig. 2(c)] also revealed the existence of bundles of rods with variable length ranging from hundreds of nanometers to few micrometers and that of diameter in the range of 50–100 nm.

Spectroscopic analysis

Fourier transform infrared (FT-IR) spectroscopic study was performed to investigate the presence of chemical bonds at the different stages of functionalization and immobilization process. Figure 3 represents the FT-IR spectra of the (i) 3-aminopropyltriethoxy saline (APTES)/WO_3 NRs/ITO (indium tin oxide), (ii) cardiac troponin I antibody (anti-cTnI)/APTES/WO_3 NRs/ITO, and (iii) ethanolamine (EA)/anti-cTnI/APTES/WO_3 NRs/ITO. The APTES/WO_3 NRs/ITO electrode exhibited characteristic bands of WO_3 at 1408 cm^{-1} and 823 cm^{-1}, which correspond to ν(W–O) and ν (W–O_{inter}–W) stretching vibration of the oxygen, respectively [27, 28]. The bands observed at 1623 and 3437 cm^{-1} indicate the presence of free –NH_2 groups in APTES molecule [29, 30]. Also, the additional band seen at 2942 cm^{-1} and 1109 cm^{-1} can be assigned to C–H bonds of aldehydes groups present on the APTES molecule surface and stretching mode of Si–O–Si, respectively [31]. After covalent immobilization of anti-cTnI, the bands observed at 1249 and 1384 cm^{-1} indicate the formation of an amide bond (C–N) between amino groups of APTES and –COOH groups of anti-cTnI. Furthermore, the bands observed at 1567 and 1643 cm^{-1} can assign to N–H bending of amide II and amide I of carbonyl stretching mode [32]. Also, few of the bands were found to be shifted on antibody immobilization. All these results indicate successful immobilization of antibody biomolecule on the functionalized matrix. Furthermore, with the incorporation of EA on the immobilized matrix, we observed no changes in the band's position, rather the intensity of the bands get reduced due to the insulating nature of EA.

Electrochemical characterizations

The electrochemical characteristics of the fabricated sensing platform were investigated using cyclic voltammetry (CV) and electrochemical impedance spectroscopic (EIS) techniques. CV has been widely studied in determining the qualitative information of electrochemical kinetics of the fabricated electrode. The cyclic voltammograms of (i) APTES/WO_3NRs/ITO,

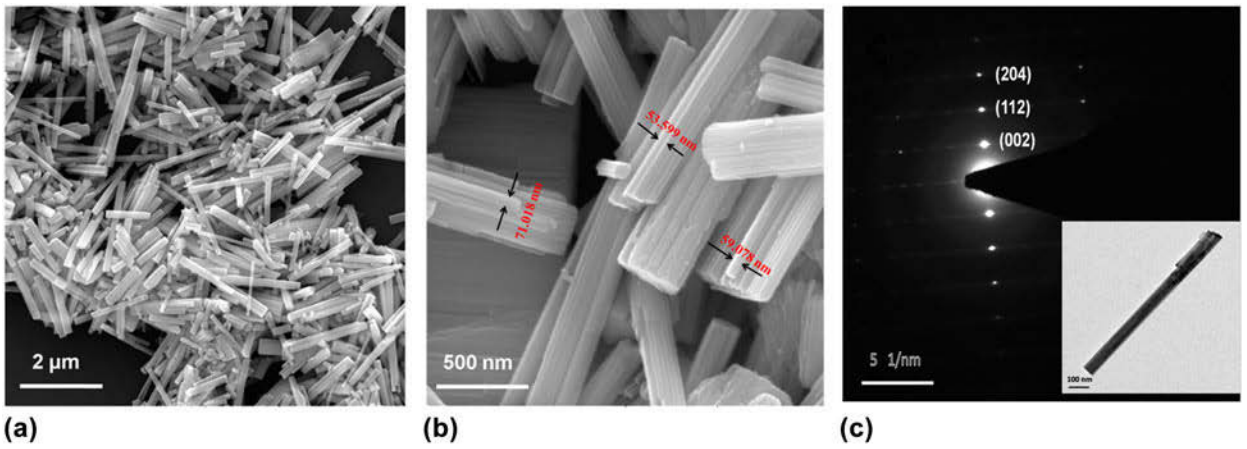

Figure 2: FESEM micrograph of WO_3 NRs (a) at low magnification and (b) at high magnification, and (c) selected area electron diffraction image of WO_3 NRs. Inset: TEM image of WO_3 NRs.

(ii) anti-cTnI/APTES/WO_3NRs/ITO, and (iii) EA/anti-cTnI/APTES/WO_3NRs/ITO, as shown in Fig. 4(a), were obtained at the scan rate of 50 mV/s in a phosphate buffered saline (PBS, pH 7.4) coupled with five millimolar $[Fe(CN)_6]^{3-/4-}$. The magnitude of the oxidation peak current to the reduction peak current (i_a/i_c = 1.05) for APTES/WO_3NRs/ITO electrode showed the reversible process of the redox couple $[Fe(CN)_6]^{3-/4-}$. Furthermore, the anodic peak current for anti-cTnI/APTES/WO_3NRs/ITO immunoelectrode (0.303 mA) was found to be lower than that for APTES/WO_3 NRs/ITO electrode (0.347 mA), indicating decreased in electron transfer at the electrode interface due to the insulating nature of the immobilized antibodies of cTnI. The incorporation of EA on immunoelectrode further decreases the magnitude of the current value to 0.230 mA. This was due to the nonspecific adsorption of EA that blocked the non-specific active sites present on the antibody immobilized surface of the immunoelectrode. All these results indicate the successful fabrication of immunosensing platform.

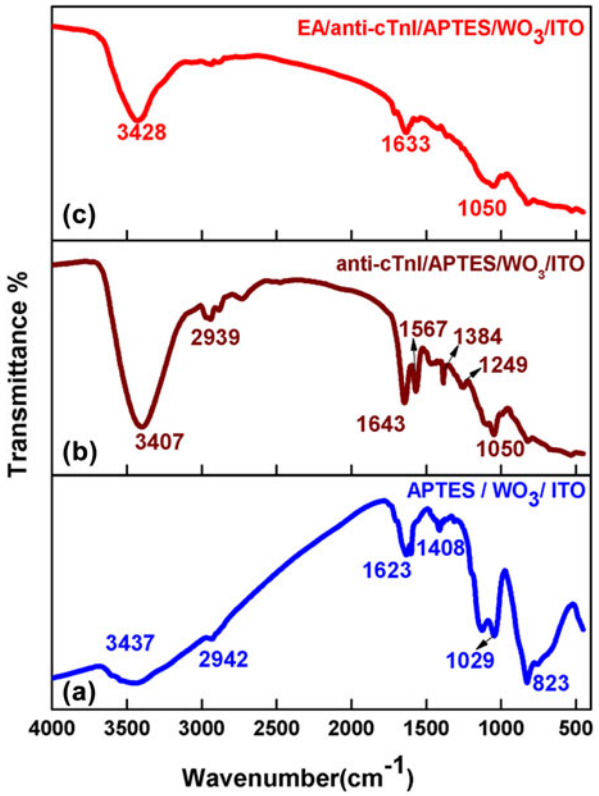

Figure 3: FT-IR spectra of (a) APTES/WO_3 NRs/ITO electrode, (b) anti-cTnI/APTES/WO_3 NRs/ITO immunoelectrode, and (c) EA/anti-cTnI/APTES/WO_3 NRs/ITO immunoelectrode.

Furthermore, the EIS study was also carried out to study the interfacial properties between the fabricated electrode surface and the electrolyte in the frequency range of 0.01–10^5 Hz. The experimental data of EIS were modeled using an equivalent circuit known as Randles circuit. The circuit consisted of Warburg impedance (Z_W), double-layer capacitance (C_{dl}), solution resistance (R_S), and the electron transfer resistance (R_{CT}). Figure 4(b) represents the EIS spectra (Nyquist plot) of the (i) APTES/WO_3NRs/ITO, (ii) anti-cTnI/APTES/WO_3NRs/ITO, and (iii) EA/anti-cTnI/APTES/WO_3 NRs/ITO immunoelectrode that was obtained on an Autolab potentiostat/galvanostat system. From the EIS spectra, the R_{CT} value of APTES/WO_3 NRs/ITO electrode was found to be 2.15 KΩ, which increased to 2.34 KΩ after antibody immobilization. This increased impedance revealed the insulating nature of the antibody. Furthermore, with the incorporation of EA molecules that covered the nonspecific sites of the immunoelectrode, the charge transfer phenomenon again gets hindered, resulting in

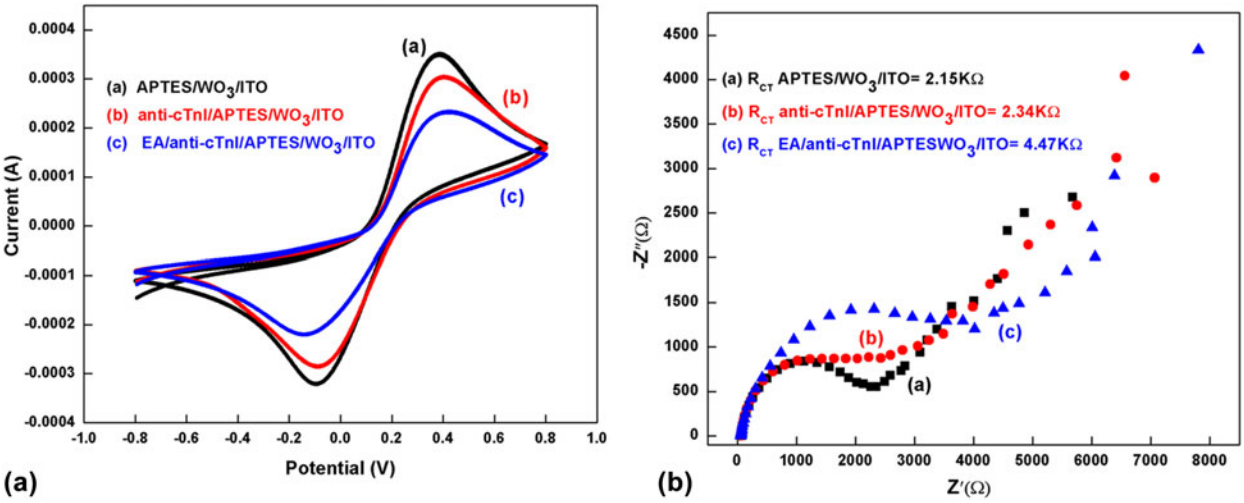

Figure 4: (a) Cyclic voltammogram (CV) of the different modified electrodes in PBS (pH = 7.4) at the scan rate of 50 mV/s. (b) The EIS spectra of the modified electrodes in the frequency range 0.01–10^5 Hz.

increase in R_{CT} value to 4.47 KΩ. Moreover, these electrodes were also characterized by evaluating heterogeneous electron transfer constant (K_O) using Eq. (2):

$$K_O = \frac{RT}{n^2F^2AR_{CT}C} \quad , \tag{2}$$

where T represents temperature, R is the gas constant, n is the total number of electrons transferring constant, F is the Faraday's constant, C is the bulk concentration of the redox couple, and A is the effective area of the electrode. The value of K_O estimated for APTES/WO_3NRs/ITO electrode (9.91×10^{-5} cm/s) was found to be high compared with that of EA/anti-cTnI/APTES/WO_3NRs/ITO immunoelectrode (4.47×10^{-5} cm/s), thus demonstrating faster electron transfer kinetics at the interface of the electrode. The cyclic voltammogram response of EA/anti-cTnI/APTES/WO_3 NRs/ITO immunoelectrode was also studied as a function of scan rate (40–160 mV/s), as shown in Fig. 5(a). The magnitude of both anodic peak current (I_{pa}) and cathodic peak current (I_{pc}) of the response exhibited a linear relationship with the square root of scan rate [Fig. 5(b)], revealing a diffusion-controlled process of the electrochemical reaction [Eqs. (3) and (4)].

$$I_{pa} = 0.022 \text{ mA} + \left[0.0287 \text{ mA(s/mV)} \times (\text{scan rate [mV/s]})^{1/2}\ R^2 = 0.0990\right] \quad , \tag{3}$$

$$I_{pc} = -0.0528 \text{ mA} + \left[-0.0225 \text{ mA(s/mV)} \times (\text{scan rate [mV/s]})^{1/2}\ R^2 = 0.0989\right] \quad . \tag{4}$$

Also, it was observed that with an increase in scan rate, there was a positive shift in the oxidation peak potential (V_{pa}) and negative shift in the reduction peak potential (V_{pc}), and linearity was seen between redox peak potential shifts ($\Delta E = V_{pa} - V_{pc}$) and the square root of the scan rate for the EA/anti-cTnI/APTES/WO_3 NRs/ITO immunoelectrode, satisfying Eq. (5). From Fig. 5(c), we observe an appreciable linear fitting, suggesting a facile electron transport from electrolyte to the electrode surface.

$$\Delta E(\text{V}) = 0.422 \text{ V} + \left[0.025 \text{ V(s/mV)} \times (\text{scan rate [mV/s]})^{1/2}\right], \quad R^2 = 0.997 \quad . \tag{5}$$

Electrochemical response investigations

The investigation of the electrochemical response studies of the fabricated immunoelectrode as a function of cTnI concentration (0.01–10 ng/mL) was performed using the EIS technique. Figure 6(a) represents the Nyquist plot of EIS performed in a PBS solution [pH = 7.4, containing $[Fe(CN)_6]^{3-/4-}$] (inset: Randles circuit). The transportation of electrochemically produced charge at the interface of electrode and electrolyte has been modeled by measuring the change in resistance. The charge transfer resistance (R_{CT}), which corresponds to the diameter of the semicircle of the Nyquist plot, has been measured using NOVA software. The R_{CT} value of the EA/anti-cTnI/APTES/WO_3 NRs/ITO immunoelectrode increased with the increase in cTnI concentration. This increase in impedance revealed the formation of insulating antigen–antibody complex produced due to the specific key–lock interaction of the anti-cTnI and cTnI, which might have hindered the electron motion. The obtained calibration plot between R_{CT} value and the cTnI concentration is shown in Fig. 6(b). The value of R_{CT} varies linearly with the cTnI concentration up to 1 ng/mL and obeys Eq. (6).

$$R_{CT} = 2.12\ (\text{K}\Omega) + 1.723\ (\text{K}\Omega \cdot \text{mL}/(\text{ng} \cdot \text{cm}^2)) \times [\text{concentration (ng/mL)}] \quad , \tag{6}$$

with regression coefficient (R^2) = 0.995.

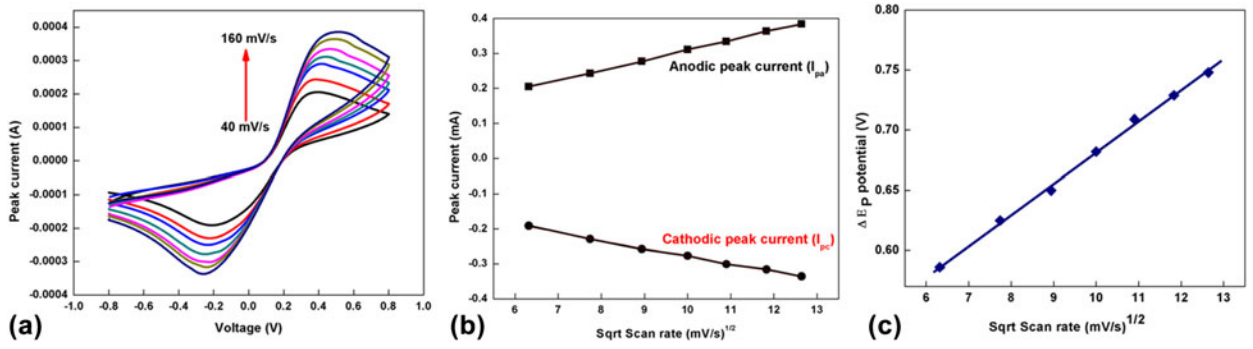

Figure 5: (a) CV response of EA/anti-cTnI/APTES/n-WO_3/ITO immunoelectrode as a function of scan rate (40–160 mV/s). (b) Variation of anodic peak current (I_{pa}) and cathodic peak current (I_{pc}) with respect to square root of the scan rate. (c) Variation of redox peak potential difference with respect to square root of scan rate.

We observed that APTES/WO_3 NRs/ITO–based immunoelectrode exhibits good sensitivity as 6.81 [KΩ·ml/(ng·cm^2)] in a linear detection range of 0.01–1 ng/mL. This high sensitivity exhibited by the immunoelectrode can be attributed to the presence of WO_3 NRs in the matrix that perhaps provided the enhanced charge conduction channel for the electron transfer kinetics. Moreover, a controlled study was conducted to investigate the electrochemical impedance response of APTES/WO_3 NRs/ITO immunoelectrode toward the cTnI antigen without using anti-cTnI [Fig. 6(b), inset]. It was found that there was no significant change in the magnitude of R_{CT} value in response to the different concentration of cTnI antigen. Hence, we can conclude that the fabricated immunosensor response was due to immunoreactions between cTnI antigen and anti-cTnI only.

The reproducibility of the EA/anti-cTnI/APTES/WO_3 NRs/ITO–based immunoelectrode was investigated by measuring the charge transfer resistance (R_{CT}) on four different fabricated immunoelectrodes prepared under ideal conditions in the presence of 0.5 ng/mL cTnI. However, no noticeable change in the R_{CT} value was observed, as seen in Fig. 7(a). The reproducibility of the immunoelectrode was estimated by evaluating relative standard deviation (RSD %). The calculated mean value of R_{CT} for these four electrodes (2.19 KΩ) with RSD of 4.14% was found to be within an acceptable error range, suggesting an excellent reproducibility of the immunoelectrode.

The selectivity study of the fabricated immunoelectrode was investigated in the presence of other interfering biomarkers, such as C-reactive protein, Mb, cytokeratin-19 antigen, and carcinoembryonic antigen, using EIS measurements. Figure 7(b) shows the interference study of the immunoelectrode, where no significant change in the R_{CT} value was observed among different interferents (concentration of each biomarker as 10 ng/mL) concerning blank immunoelectrode. However, after addition of cTnI antigen, there was a remarkable change in the R_{CT} value, which signifies the high specificity of the fabricated immunoelectrode for the cTnI biomarker.

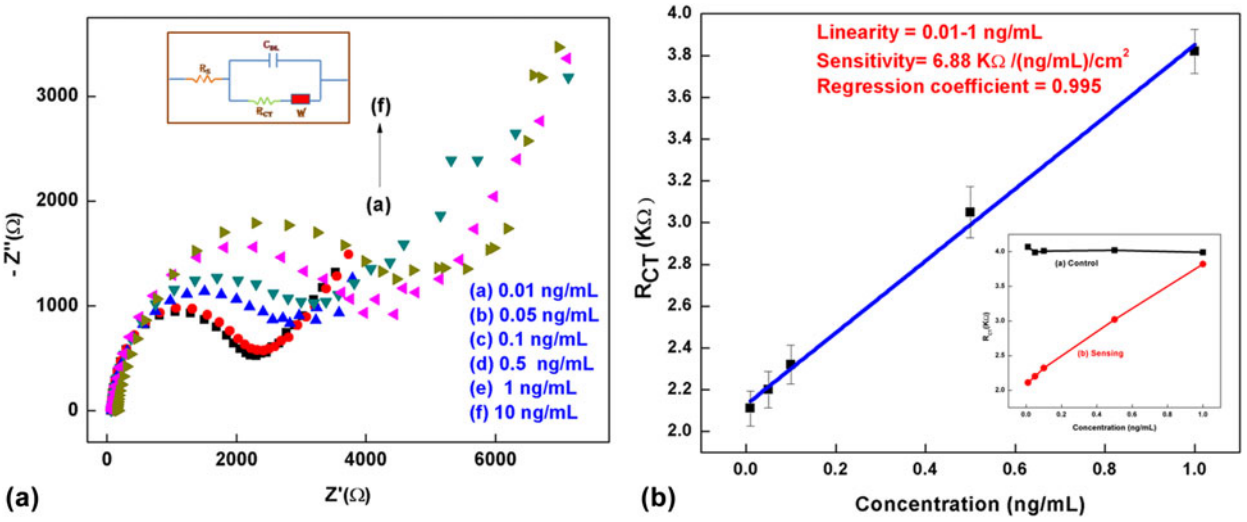

Figure 6: (a) EIS response study of the immunoelectrode as a function of cTnI antigen concentration (0.01–10 ng/mL); inset shows Randles equivalent circuit. (b) A calibration plot obtained between R_{CT} and cTnI antigen concentration; inset shows sensing along with control study.

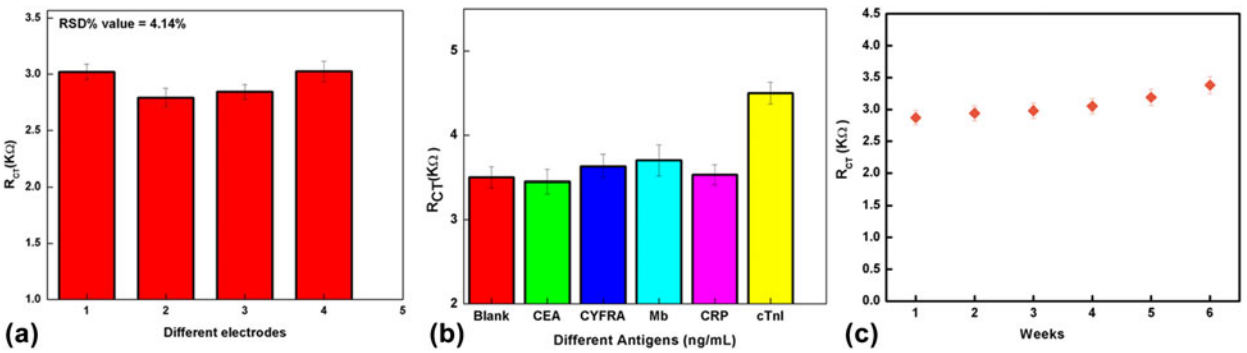

Figure 7: (a) Reproducibility study of the immunoelectrodes fabricated under identical conditions with cTnI (0.5 ng/mL). (b) Interference study of the immunoelectrode in the presence of different interferents. (c) Shelf life study of the EA/anti-cTnI/APTES/nWO_3/ITO immunoelectrode.

Furthermore, the shelf life study of the fabricated immunoelectrode was conducted by measuring R_{CT} value in the presence of 0.5 ng/mL cTnI antigen at the regular interval of 7 days [Fig. 7(c)]. The increase in R_{CT} value was found to be 7.3% up to 5 weeks after which the R_{CT} increased to more than 20% at the end of 6 weeks. Thus, the fabricated immunoelectrode retained its biological activity up to 5 weeks. Hence, all these results indicated that the EIS technique for detection of biomarkers proved to be an efficient, simple, and fast response technique. In Table I, the sensing characteristics of the fabricated immunosensor are compared with those of other reported in the literature.

Conclusion

We have developed an efficient and a label-free electrochemical sensing platform for detection of cardiac biomarker using nWO_3 NRs as an immobilized matrix. The APTES-functionalized WO_3 NRs were deposited on ITO electrode using electrophoretic deposition (EPD) technique, and subsequently, the functionalized WO_3 NRs were used as an immobilized matrix for the covalent binding of anti-cTnI biomolecules. The variation in impedance signal of the fabricated immunosensor was observed on formation of immunocomplex between anti-cTnI and cTnI antigen. The experimental results of the impedimetric studies reveal high sensitivity [6.81 KΩ·ml/(ng·cm^2)] and good reproducibility with long-term stability (5 weeks). The better performance of the proposed immunosensor can be attributed to the enhanced electrochemical and high electrocatalytic activity of WO_3 NRs, which provide high aspect ratio for increased antibody loading onto WO_3 NRs matrix. Hence, these results direct us toward the realization of integrated and portable POC diagnostic tool based on WO_3 NRs matrix.

Experimental

Materials and reagents

Sodium tungstate ($Na_2WO_4{\cdot}2H_2O$), NaCl, and HCl were used as reagents for the synthesis of WO_3 NRs. APTES, water-soluble EDC [1-(3-(dimethylamino)-propyl)-3-ethylcarbodiimide hydrochloride], EA, and *N*-hydroxysulfosuccinimide (NHS) were used for the functionalization and immobilization process and were procured from Sigma–Aldrich and Fisher Scientific. Potassium ferricyanide $K_3[Fe(CN)_6]$ and potassium ferrocyanide $K_4[Fe(CN)_6]{\cdot}3H_2O$ were also procured from Fisher Scientific. cTnI antigen and anti-cTnI were obtained from Ray Biotech, Inc. (India). PBS (pH 7.4) solution was used for the dilution of biomolecules and washing, and it was prepared using sodium monophosphate (NaH_2PO_4, 0.02 mol/L) and sodium diphosphate dihydrate ($Na_2HPO_4{\cdot}2H_2O$, 0.02 mol/L), which were procured from Fisher Scientific. All the reagents and chemicals were used without any further purification. The Milli-Q water having a resistivity of 18.3 MΩ was used for the preparation of all buffers and solutions.

Instrumentation

The crystallography of the as-synthesized material was studied using powder XRD analyzer obtained on a Bruker D-8 Advances equipped with Cu K_α radiation wavelength, λ = 0.154 nm. The morphological and structural studies were investigated using FESEM (TESCAN), TEM (JEOL), and FT-IR spectrometer (PerkinElmer). The CV and EIS studies were carried out at ambient temperature (24 °C) on an Autolab Potentiostat (the Netherlands) using NOVA software. The standard three-electrode cell configuration was used for conducting the electrochemical measurements with the fabricated electrode as the working electrode, platinum (Pt) wire as the counter electrode, and silver/silver chloride (Ag/AgCl) electrode as the reference electrode. PBS solution (50 mM, pH 7.4) containing 5 mM of $[Fe(CN)_6^{3-/4-}]$ as redox species was used as an electrolyte.

Synthesis and functionalization of WO_3 NRs

Synthesis of WO_3 NRs

nWO_3 was synthesized using a hydrothermal method. First, 0.5 M sodium tungstate ($Na_2WO_4{\cdot}2H_2O$) solution was prepared in 30 mL of Milli-Q water and was stirred continuously. The pH value of the resultant solution was reduced to "2" with the addition of 6 M HCl dropwise. Further 1.2 g of NaCl was added to the solution and stirred for two hours. After two hours, the resultant solution was transferred to a 50-mL Teflon-lined vessel and placed in a stainless steel autoclave. This autoclave was then placed in an oven at 180 °C for about

TABLE I: Sensing characteristics of the WO_3 NR–based platform compared with those reported in the literature.

Sensing platform	Detection technique	Label	Detection range	Sensitivity (*S*)	Detection limit	Stability	Reference
ZnO n.ps	FET	No	1 ng/mL–10 μg/mL	35.3 nA/(g/mL)	3.24 pg/mL	...	[34]
Gold nanodumbbells	EIS	...	0.05–500 ng/mL	...	8 pg/mL	...	[35]
Carbon nanofibers	EIS	No	0.25–10 ng/mL	...	0.2 ng/mL	...	[36]
ZrO_2 n.ps	CV	No	0.1–100 ng/mL	3.9 μA·mL/(ng·cm^2)	0.1 ng/mL	...	[26]
WO_3 NRs	EIS	No	0.01–10 ng/mL	6.81 [KΩ·mL/(ng·cm^2)]	0.01 ng/mL	5 weeks	Present work

10 h for hydrothermal reaction. After this reaction period, the stainless steel autoclave was allowed to cool naturally to room temperature, and the sample was collected after centrifuging it 4–5 times with Milli-Q water. The as-synthesized sample was used for further characterization and functionalization process.

Functionalization and preparation of electrodes

The as-synthesized nanostructures were chemically modified to activate functional groups on their surfaces for the immobilization of the biomolecules. APTES is an amino-silane compound that customarily provides active amino groups ($-NH_2$) that can covalently bond with carboxyl groups (–COOH) of the antibody biomolecules [33]. APTES was thus used for the functionalization process. In brief, 100 mg of WO_3 NRs was dispersed in 30 mL of 2-propanol and sonicated to obtain a well-dispersed suspension. Next, 250 µL of APTES (98%) was added to the suspended solution and was stirred at 280 rpm for 40 h at room temperature (24 °C). The resultant functionalized WO_3 NRs were filtered and washed thoroughly with Milli-Q water to remove the unbound APTES. EPD technique was employed for the deposition of functionalized WO_3 NRs (APTES/WO_3 NRs) onto ITO glass substrate. Before deposition, a highly dispersed colloidal suspension of functionalized WO_3 NRs (1 mg/mL) was prepared in acetonitrile via ultrasonication. An optimized DC potential (48 V) for 120 s was considered for the deposition of the APTES/WO_3 NRs film onto the hydrolyzed ITO electrode using a two-electrode system, where a hydrolyzed ITO and platinum wire were taken as an anode and a cathode, respectively. Finally, the as-prepared electrode (APTES/WO_3NRs/ITO) was washed with Milli-Q water and kept in a covered Petri dish for further modifications.

Fabrication of immunosensor

For immobilization of anti-cTnI, 20 µL of anti-cTnI solution (see supplementary sheet) was uniformly spread on the surface of the APTES/WO_3 NRs/ITO electrode by drop casting. The prepared electrode was kept in a humid chamber at room temperature for 6–7 h. The $-NH_2$ groups of APTES molecules can be covalently bound with –COOH groups of anti-cTnI that were activated using EDC and NHS chemistry, resulting in the formation of a strong amide bond (OC–NH). Last, EA (0.01 M) was used for blocking the all nonspecific active sites of the fabricated electrode. The resulting EA/anti-cTnI/APTES/WO_3 NRs/ITO immunosensor was kept at 5 °C when not in use. A stepwise fabrication of immunosensor and immobilization of antibodies on the surface of APTES/WO_3 NRs/ITO electrode is shown in Scheme 1.

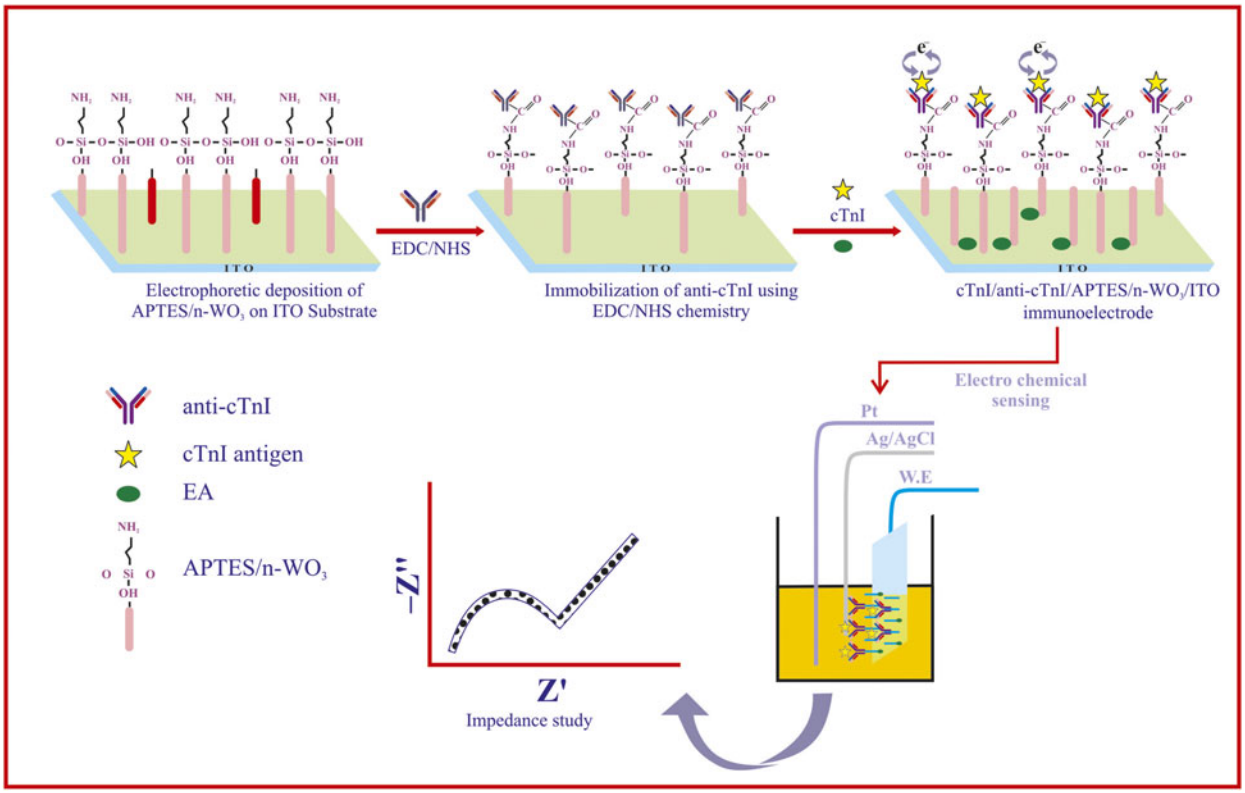

Scheme 1: Schematic representation of fabrication of immunoelectrode for electrochemical biosensing.

References

1. **P.R. Solanki, A. Kaushik, V.V. Agrawal, and B.D. Malhotra**: Nanostructured metal oxide-based biosensors. *NPG Asia Mater.* **3**, 17 (2011).
2. **A. Walcarius, S.D. Minteer, J. Wang, Y. Lin, and A. Merkoçi**: Nanomaterials for bio-functionalized electrodes: Recent trends. *J. Mater. Chem. B* **1**, 4878 (2013).
3. **F. Wang, L. Song, H. Zhang, L. Luo, D. Wang, and J. Tang**: One-dimensional metal-oxide nanostructures for solar photocatalytic water-splitting. *J. Electron. Mater.* **46**, 4716 (2017).
4. **X. Fang, L. Hu, C. Ye, and L. Zhang**: One-dimensional inorganic semiconductor nanostructures: A new carrier for nanosensors. *Pure Appl. Chem.* **82**, 2185 (2010).
5. **P.R. Solanki, J. Singh, B. Rupavali, S. Tiwari, and B.D. Malhotra**: Bismuth oxide nanorods based immunosensor for mycotoxin detection. *Mater. Sci. Eng., C* **70**, 564 (2017).
6. **P. Galvin, N. Padmanathan, K.M. Razeeb, J.F. Rohan, L.C. Nagle, A. Wahl, E. Moore, W. Messina, K. Twomey, and V. Ogurtsov**: Nanoenabling electrochemical sensors for life sciences applications. *J. Mater. Res.* **32**, 2883 (2017).
7. **S. Augustine, A.G. Joshi, B.K. Yadav, A. Mehta, P. Kumar, V. Renugopalakrishanan, and B.D. Malhotra**: An emerging nanostructured molybdenum trioxide-based biocompatible sensor platform for breast cancer biomarker detection. *MRS Commun.* **8**, 668 (2018).
8. **Y. Zhao, X. Yan, Z. Kang, X. Fang, X. Zheng, L. Zhao, H. Du, and Y. Zhang**: Zinc oxide nanowires-based electrochemical biosensor for L-lactic acid amperometric detection. *J. Nanopart. Res.* **16**, 2398 (2014).
9. **C. Yan, W. Kang, J. Wang, M. Cui, X. Wang, C.Y. Foo, K.J. Chee, and P.S. Lee**: Stretchable and wearable electrochromic devices. *ACS Nano* **8**, 316 (2013).
10. **I.M. Szilágyi, B. Fórizs, O. Rosseler, Á. Szegedi, P. Németh, P. Király, G. Tárkányi, B. Vajna, K. Varga-Josepovits, and K. László**: WO_3 photocatalysts: Influence of structure and composition. *J. Catal.* **294**, 119 (2012).
11. **D. Sandil, S. Kumar, K. Arora, S. Srivastava, B. Malhotra, S. Sharma, and N.K. Puri**: Biofunctionalized nanostructured tungsten trioxide based sensor for cardiac biomarker detection. *Mater. Lett.* **186**, 202 (2017).
12. **H. Zheng, Y. Tachibana, and K. Kalantar-zadeh**: Dye-sensitized solar cells based on WO_3. *Langmuir* **26**, 19148 (2010).
13. **J. Shi, G. Hu, Y. Sun, M. Geng, J. Wu, Y. Liu, M. Ge, J. Tao, M. Cao, and N. Dai**: WO_3 nanocrystals: Synthesis and application in highly sensitive detection of acetone. *Sens. Actuators, B* **156**, 820 (2011).
14. **L. Santos, C.M. Silveira, E. Elangovan, J.P. Neto, D. Nunes, L. Pereira, R. Martins, J. Viegas, J.J. Moura, and S. Todorovic**: Synthesis of WO_3 nanoparticles for biosensing applications. *Sens. Actuators, B* **223**, 186 (2016).
15. **Z-X. Cai, H-Y. Li, J-C. Ding, and X. Guo**: Hierarchical flowerlike WO_3 nanostructures assembled by porous nanoflakes for enhanced NO gas sensing. *Sens. Actuators, B* **246**, 225 (2017).
16. **Y. Zhou, L. Yang, S. Li, and Y. Dang**: A novel electrochemical sensor for highly sensitive detection of bisphenol A based on the hydrothermal synthesized Na-doped WO_3 nanorods. *Sens. Actuators, B* **245**, 238 (2017).
17. **J. Liu, O. Margeat, W. Dachraoui, X. Liu, M. Fahlman, and J. Ackermann**: Gram-scale synthesis of ultrathin tungsten oxide nanowires and their aspect ratio-dependent photocatalytic activity. *Adv. Funct. Mater.* **24**, 6029 (2014).
18. **J. Ali, J. Najeeb, M.A. Ali, M.F. Aslam, and A. Raza**: Biosensors: Their fundamentals, designs, types and most recent impactful applications: A review. *J. Biosens. Bioelectron.* **8**, 1 (2017).
19. **S. Ko, B. Kim, S-S. Jo, S.Y. Oh, and J-K. Park**: Electrochemical detection of cardiac troponin I using a microchip with the surface-functionalized poly(dimethylsiloxane) channel. *Biosens. Bioelectron.* **23**, 51 (2007).
20. **M.D. Prakash, S. Singh, C. Sharma, and V.S.R. Krishna**: Electrochemical detection of cardiac biomarkers utilizing electrospun multiwalled carbon nanotubes embedded SU-8 nanofibers. *Electroanalysis* **29**, 380 (2017).
21. **N.J. Ronkainen, H.B. Halsall, and W.R. Heineman**: Electrochemical biosensors. *Chem. Soc. Rev.* **39**, 1747 (2010).
22. **B.D. Malhotra, S. Srivastava, M.A. Ali, and C. Singh**: Nanomaterial-based biosensors for food toxin detection. *Appl. Biochem. Biotechnol.* **174**, 880 (2014).
23. **A. Qureshi, Y. Gurbuz, and J.H. Niazi**: Biosensors for cardiac biomarkers detection: A review. *Sens. Actuators, B* **171**, 62 (2012).
24. **X. Han, S. Li, Z. Peng, A.M. Othman, and R. Leblanc**: Recent development of cardiac troponin I detection. *ACS Sens.* **1**, 106 (2016).
25. **T. Keller, T. Zeller, D. Peetz, S. Tzikas, A. Roth, E. Czyz, C. Bickel, S. Baldus, A. Warnholtz, and M. Fröhlich**: Sensitive troponin I assay in early diagnosis of acute myocardial infarction. *N. Engl. J. Med.* **361**, 868 (2009).
26. **S. Kumar, S. Kumar, S. Augustine, and B.D. Malhotra**: Protein functionalized nanostructured zirconia based electrochemical immunosensor for cardiac troponin I detection. *J. Mater. Res.* **32**, 2966 (2017).
27. **W. Zhao, B. Cui, H. Qiu, P. Chen, and Y. Wang**: Multifunctional Fe_3O_4@WO_3@mSiO_2–APTES nanocarrier for targeted drug delivery and controllable release with microwave irradiation triggered by WO_3. *Mater. Lett.* **169**, 185 (2016).
28. **M. Tong, G. Dai, Y. Wu, X. He, and D. Gao**: WO_3 thin film prepared by PECVD technique and its gas sensing properties to NO_2. *J. Mater. Sci.* **36**, 2535 (2001).
29. **D. Sandil, S. Srivastava, B. Malhotra, S. Sharma, and N.K. Puri**: Biofunctionalized tungsten trioxide-reduced graphene oxide nanocomposites for sensitive electrochemical immunosensing of cardiac biomarker. *J. Alloys Compd.* **763**, 102–110 (2018).

30. **N. Majoul, S. Aouida, and B. Bessaïs**: Progress of porous silicon APTES-functionalization by FTIR investigations. *Appl. Surf. Sci.* **331**, 388 (2015).
31. **M. Ata, Y. Liu, and I. Zhitomirsky**: A review of new methods of surface chemical modification, dispersion and electrophoretic deposition of metal oxide particles. *RSC Adv.* **4**, 22716 (2014).
32. **S. Srivastava, S. Abraham, C. Singh, M.A. Ali, A. Srivastava, G. Sumana, and B.D. Malhotra**: Protein conjugated carboxylated gold@reduced graphene oxide for aflatoxin B_1 detection. *RSC Adv.* **5**, 5406 (2015).
33. **S. Kumar, S. Kumar, S. Tiwari, S. Augustine, S. Srivastava, B.K. Yadav, and B.D. Malhotra**: Highly sensitive protein functionalized nanostructured hafnium oxide based biosensing platform for non-invasive oral cancer detection. *Sens. Actuators, B* **235**, 1 (2016).
34. **M. Fathil, M.M. Arshad, A. Ruslinda, S.C. Gopinath, R. Adzhri, U. Hashim, and H. Lam**: Substrate-gate coupling in ZnO-FET biosensor for cardiac troponin I detection. *Sens. Actuators, B* **242**, 1142 (2017).
35. **M. Negahdary, M. Behjati-Ardakani, N. Sattarahmady, H. Yadegari, and H. Heli**: Electrochemical aptasensing of human cardiac troponin I based on an array of gold nanodumbbells—Applied to early detection of myocardial infarction. *Sens. Actuators, B* **252**, 62 (2017).
36. **A. Periyakaruppan, R.P. Gandhiraman, M. Meyyappan, and J.E. Koehne**: Label-free detection of cardiac troponin-I using carbon nanofiber based nanoelectrode arrays. *Anal. Chem.* **85**, 3858 (2013).